CHEMISTRY
A EUROPEAN JOURNAL

FULL PAPER

DOI: 10.1002/chem.201200883

Hydrogen Bonding Directed Supramolecular Polymerisation of Oligo(Phenylene-Ethynylene)s: Cooperative Mechanism, Core Symmetry Effect and Chiral Amplification

Feng Wang, Martijn A. J. Gillissen, Patrick J. M. Stals, Anja R. A. Palmans,* and E. W. Meijer*[a]

Abstract: The design of supramolecular motifs with tuneable stability and adjustable supramolecular polymerisation mechanisms is of crucial importance to precisely control the properties of supramolecular assemblies. This report focuses on constructing π-conjugated oligo(phenylene ethynylene) (OPE)-based one-dimensional helical supramolecular polymers that show a cooperative growth mechanism. Thus, a novel set of discotic molecules comprising a rigid OPE core, three amide groups, and peripheral solubilising wedge groups featuring C_3 and C_2 core symmetry was designed and synthesised. All of the discotic molecules are crystalline compounds and lack a columnar mesophase in the solid state. In dilute methylcyclohexane solution, one-dimensional supramolecular polymers are formed stabilised by threefold intermolecular hydrogen bonding and π–π interactions, as evidenced by ^{1}H NMR measurements. Small-angle X-ray and light scattering measurements reveal significant size differences between the columnar aggregates of C_3- and C_2-symmetrical discotics, that is, the core symmetry strongly influences the nature of the supramolecular polymerisation process. Temperature-dependent CD measurements show a highly cooperative polymerisation process for the C_3-symmetrical discotics. In contrast, the self-assembly of C_2-symmetrical discotics shows a smaller enthalpy release upon aggregation and decreased cooperativity. In all cases, the peripheral stereogenic centres induce a preferred handedness in the columnar helical aggregates. Moreover, one stereogenic centre suffices to fully bias the helicity in the C_2-symmetrical discotics. Finally, chiral amplification studies with the C_3-symmetrical discotics were performed by mixing chiral and achiral discotics (sergeants-and-soldiers experiment) and discotics of opposite chirality (majority-rules experiment). The results demonstrate a very strong sergeants-and-soldiers effect and a rather weak majority-rules effect.

Keywords: cooperative effects · helical structures · polymerization · self-assembly · supramolecular chemistry

Introduction

Over the past decades, extensive research has been devoted to the bottom-up self-assembly of π-conjugated systems into one-dimensional helical objects, for the development of conducting materials with future applications in the fields of sensing, imaging, and optoelectronic devices.[1] Although π-conjugated molecules exhibit an intrinsic ability to self-assemble into extended structures, more precise control of the dimensionality and helicity towards well-defined nanoarchitectures is still keenly pursued. Introduction of hydrogen bonding in π-conjugated systems is an especially promising strategy, since the highly selective and directional hydrogen bonding could increase the binding strength of π-conjugated molecules, provide enhanced stability to the assemblies, and position the π-conjugated molecules in a desired arrangement.[2] Up to now, various types of π-conjugated systems, such as triphenylene, tetrathiafulvalene, porphyrin, phthalocyanine, oligophenylenevinylene and oligofluorene have been incorporated successfully with hydrogen bonding motifs,[3] which led to intriguing properties for the resulting π-functional materials.

Oligo(phenylene-ethynylene)s, OPEs, are another type of rigid π-conjugated systems and have some superior properties. First, OPEs could serve as molecular wires due to their planar conformation resulting in lower energy for the electronic transitions between the chromophores, which is highly important for improving the performance of optoelectronic devices.[4] Second, the rotational conformational heterogeneity of the OPEs induces a unidirectional switching process, which is promising for the development of stimuli-responsive materials.[5] Third, the OPEs could act as precursors for a variety of metal alkynyl compounds, which

---

[a] Dr. F. Wang, M. A. J. Gillissen, P. J. M. Stals, Dr. A. R. A. Palmans,
Prof. Dr. E. W. Meijer
Institute for Complex Molecular Systems
Laboratory of Macromolecular and Organic Chemistry
Eindhoven University of Technology, PO Box 513
5600 MB Eindhoven (The Netherlands)
Fax: (+31) 402-451-036
E-mail: A.Palmans@tue.nl
E.W.Meijer@tue.nl

Supporting information for this article is available on the WWW under http://dx.doi.org/10.1002/chem.201200883.

demonstrate outstanding applications in the areas of electrical conductivity, gas storage and nonlinear optics.[6] In addition, OPEs have found a number of applications in the field of chemical actuators and sensors.[7] However, comparatively little effort has been devoted to utilizing hydrogen bonding as a tool to program the self-assembly of OPEs into ordered superstructures.[8] Recently, Sanchez and co-workers prepared a series of OPE-based discotic compounds containing three amide groups, the cooperative self-assembly and pronounced chirality amplification of which highlight the impact of hydrogen bonding in π-conjugated systems. It is of paramount importance to establish π-conjugated assemblies with a cooperative mechanism,[9] since the cooperative polymerisation process avoids the formation of many small oligomers as compared to its isodesmic counterpart.

We have extensively studied the cooperative supramolecular polymerisation of C_3-symmetrical benzene-1,3,5-tricarboxamides (BTAs) into one-dimensional helical aggregates in the past years.[10] Here we integrate the internal π-conjugated OPE core with the BTA structure to afford novel N-centred C_3-symmetrical discotic tris-amides **1**–**3** (Figure 1). The marriage of the conjugated OPEs with amide groups rebalances the interplay between the noncovalent π–π stacking and hydrogen-bonding interactions. Hence, it raises the question whether the introduction of different noncovalent interactions can significantly affect the supramolecular polymerisation mechanism. Furthermore, we evaluate the impact of desymmetrisation of the discotic structure on the properties of the supramolecular polymers. Desymmetrisation, which is important for enabling future functionalisation,[11] is mainly performed in most discotics by altering the peripheral substituents while leaving the core intact.[11a–c] We are interested in altering the core structure of C_3-symmetrical discotics **1**–**3**, since such modification would lead to a different molecular arrangement within the aggregates. Hence, to evaluate the effect of reduced core symmetry on the self-assembly properties, we designed C_2-symmetrical discotic tris-amide (*S*)-**4** (Figure 1). Comparison with C_3-symmetrical discotics reveals the correlations among core-symmetry effect, supramolecular mechanism and properties of the resulting aggregates, which would be advantageous for establishment of structure–property relationships of such discotic compounds. Ultimately, by combination of experimental techniques with theoretical analysis, we aim to quantitatively probe the contributions of the different noncovalent interactions and get deeper insight into the molecular parameters that govern supramolecular polymerisation.

Results and Discussion

Design and synthesis: The C_3-symmetrical OPE-based discotics **1**–**3** comprise star-shaped OPEs as the core and three N-centred amide groups, affording π–π stacking and hydrogen-bonding interactions, respectively. Three wedge groups at the periphery are introduced to enhance the solubility in apolar solvents. The chiral 3,7-dimethyloctyl substituents in (*S*)-**2** and (*R*)-**3** are anticipated to induce a helical bias in the resulting supramolecular assemblies, which allows investigation of chiral amplification by mixing achiral and chiral discotics. On the other hand, only one stereogenic centre is attached at the periphery of C_2-symmetrical discotic tris-amide (*S*)-**4** in order to avoid diastereomeric mixtures.

The synthetic route to the desired discotic tris-amides **1**–**4** is straightforward (Scheme 1). Reaction of 4-iodoaniline with the appropriate trialkoxybenzoic acid in the presence of *N*-(3-dimethylaminopropyl)-*N*′-ethylcarbodiimide hydrochloride (EDC) and 4-dimethylaminopyridine (DMAP) yielded the corresponding amides **5a**–**c**, which were further coupled with 1,3,5-triethynylbenzene or (*S*)-2,7-dimethyloctyl-3,5-diethynylbenzamide by utilizing a

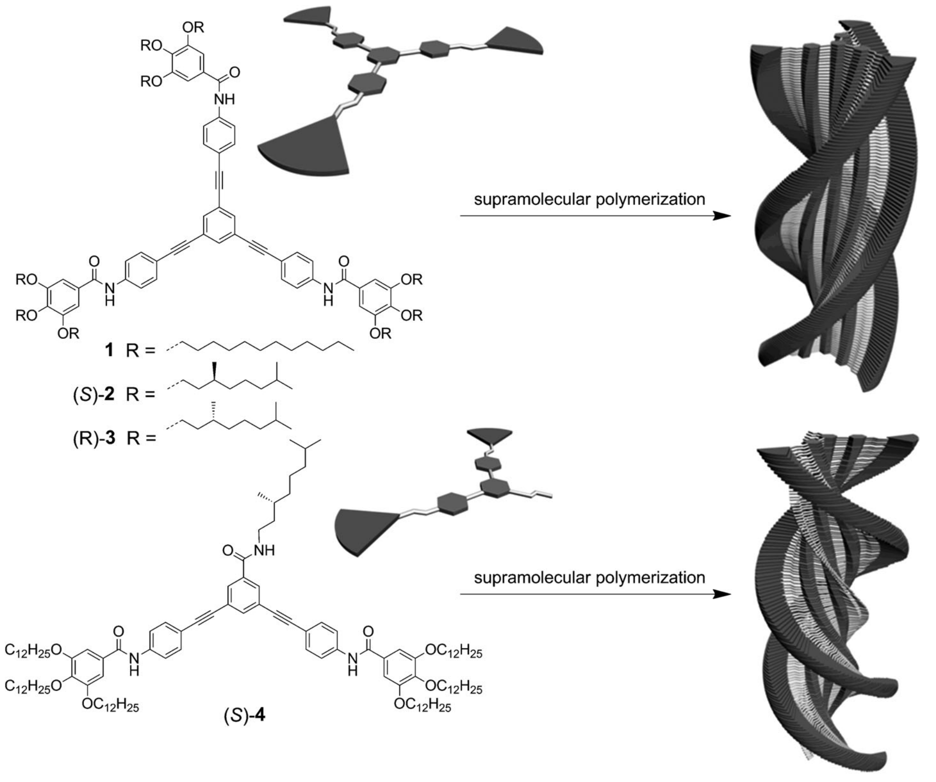

Figure 1. Structures of discotic tris-amides **1**–**4** and schematic representation of the cooperative supramolecular polymerisation process into helical stacks.

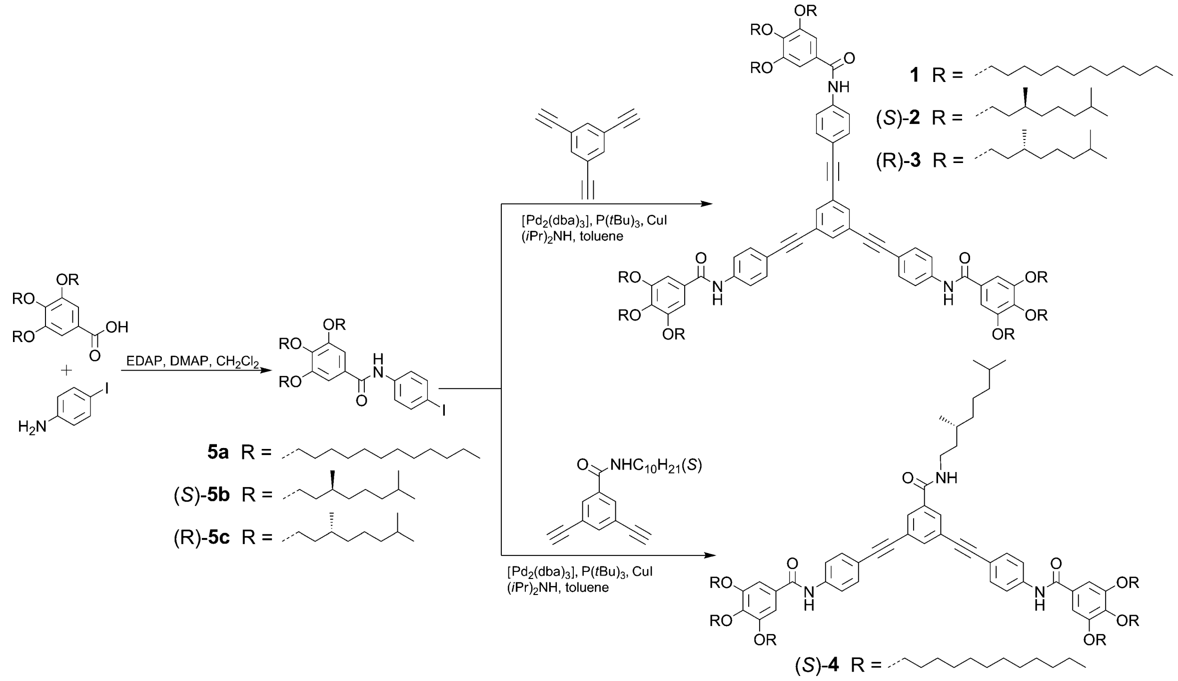

Scheme 1. Synthesis of discotic tris-amides **1**–**4**.

Sonogashira cross-coupling reaction to afford the four desired compounds **1**–**4**. P*t*Bu$_3$ was used as the ligand in the Sonogashira reaction to overcome the steric repulsion problems exerted by the wedge group, which would significantly decrease the yield of the reaction.[12] The proposed structures of the target compounds were confirmed by the NMR and MALDI-TOF mass spectra (see Supporting Information, Figures S1–S6).

Solid-state properties of discotic tris-amides 1–4: The thermal behaviour of discotic tris-amides **1**–**4** was studied by differential scanning calorimetry (DSC) and polarised optical microscopy (POM). The thermal transitions obtained from the second DSC heating run (Supporting Information, Figure S7) are summarised in Table 1. All discotic compounds **1**–**4** show a crystal-to-isotropic transition and lack a columnar mesophase, quite different from previously reported BTAs.[10c,d] When comparing compounds **1** and **4**, in which one OPE group is replaced by a branched alkylamide chain, a significant reduction in the melting temperature from 196 to 48.1 °C is observed, indicative of the impact of reduced symmetry on the melting behaviour of OPE-based discotics. The morphology of the samples upon cooling from the isotropic phase was further investigated by POM measurements under crossed polarisers (Supporting Information, Figure S8). All samples display birefringent, immobile textures characteristic of a crystalline state. Interestingly, linear compound **1** exhibits a liquid-crystalline phase from 190 °C to 196 °C in the first heating run in POM and DSC (Supporting Information, Figure S2a). However, the transition at 190 °C does not reappear in the cooling or second heating run.

Fourier transform IR spectroscopy is a sensitive technique to investigate the hydrogen-bonding interactions between the neighbouring amide groups, since the formation of lateral hydrogen bonds lowers the vibrational energy of the amide group. In the C=O-centred OPE-based discotics studied by Sanchez and co-workers, columnar structures stabilised by threefold intermolecular hydrogen bonding were assigned and characterised by well-defined bands at 3280 (NH stretch), 1635 (amide I) and 1545 cm^{-1} (amide II).[8d] The FTIR data of discotic tris-amides **1**–**4** at room temperature are summarised in Table 1 (see Supporting Information, Figure S9 for full spectra). For C_3-symmetrical compounds **1**–**3**, the NH stretching peak is broadened and located at about 3280 cm^{-1}, while a split C=O stretching band is observed at approximately 1646 and 1578 cm^{-1} and the amide II band at about 1510 cm^{-1}. The C_2-symmetrical compound (*S*)-**4** exhibits similar IR bands to **1**–**3**, except that the NH stretching vibration is located at a higher wavenumber of 3301 cm^{-1}, suggesting weaker intermolecular

Table 1. DSC and IR data of discotic tris-amides **1**–**4** in the solid state.

Compound	T [°C][a] (ΔH [kJ mol^{-1}])	$\tilde{\nu}_{(\mathrm{N-H})}$ [cm^{-1}][b]	$\tilde{\nu}_{(\mathrm{C=O})}$ [cm^{-1}][b]	$\tilde{\nu}_{(\text{amide II})}$ [cm^{-1}][b]
1	K 196.2 (43.4) I	3279	1646, 1578	1510
(*S*)-**2**	K 178.6 (40.3) I	3288	1647, 1578	1510/1495
(*R*)-**3**	K 178.7 (41.1) I	3288	1646, 1578	1509/1495
(*S*)-**4**	K 48.1 (4.7) I	3301	1644, 1580	1545/1495

[a] DSC data were derived from the second heating run. [b] The IR data were obtained at room temperature from the solid materials.

hydrogen bonding than the C_3-symmetrical analogues.

We recorded variable-temperature IR spectra of (*S*)-**2** and (*S*)-**4**, to investigate the effect of temperature on the hydrogen-bonding strength. Based on the above DSC measurement, (*S*)-**2** is a crystalline solid that melts at 178 °C. The IR spectra remain identical up to the melting point. At 200 °C the NH stretch is shifted to a higher wavenumber of 3329 cm^{-1}, and the C=O stretch at 1647 cm^{-1} is split into two peaks, one of which corresponds to the unbound C=O vibration (Figure 2). Observation of similar phenomena for (*S*)-**4** (Supporting Information, Figure S10) suggests that the hydrogen bonding is significantly weakened and disordered for the discotic tris-amides at high temperature. Despite the clear indications of hydrogen bonding between the amide groups of discotic tris-amides **1**–**4** in the solid state, we have no evidence for the formation of columnar structures stabilised by threefold hydrogen bonding. For a similar example in the literature, formation of 2D sheetlike assemblies from a large π-conjugated monomer to maximize the π–π interactions in the solid state was reported.[13] Unfortunately, crystal structures of the OPE-based discotic tris-amides could not be obtained to validate this hypothesis.

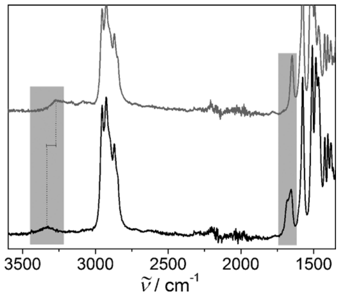

Figure 2. Variable-temperature IR spectra of (*S*)-**2** at 30 °C (grey line) and 200 °C (black line). The shaded rectangles indicate the NH (left) and C=O (right) stretching regions, respectively.

Structural characterisation of the discotic tris-amides in solution: Since solvent molecules provide energetically favourable contact with the discotic molecules, we investigated the self-assembly of **1**–**4** in solution. The presence of hydrogen-bonding and π–π stacking interactions in combination with solvophobic effects could induce the discotic tris-amides **1**–**4** to self-assemble in elongated, columnar aggregates in solution. Therefore, laser light scattering (LLS) and small-angle X-ray scattering (SAXS) were carried out to investigate the morphology of the resulting supramolecular polymers.

Dynamic light scattering measurements (DLS) were performed on C_3-symmetrical discotic tris-amide **1** and C_2-symmetrical discotic tris-amide (*S*)-**4** at a concentration of 10^{-4} M in methylcyclohexane (MCH). While the DLS results for **1** are indicative of elongated structures in solution (see Supporting Information, Figure S11), the scattered light intensity of (*S*)-**4** was too low to gain size information, probably due to the small size of the aggregates. SAXS profiles obtained at a higher concentration of 10^{-3} M in MCH clearly show the difference in the scattering curves between **1** and (*S*)-**4** (Figure 3). The q^{-1} slope in the scattered intensity for **1** is typical for elongated structures, whereas the q^0 slope found for (*S*)-**4** is indicative of spherical aggregates. Figure 3 shows an excellent agreement between the data of **1** and a fit using a cylindrical form factor with $R = 1.82$ nm and $L > 52$ nm, while the data of (*S*)-**4** fit well to a spherical form factor with $R = 1.52$ nm. At 10^{-4} M, SAXS and static light scattering (SLS) reveal a q^{-1} slope in the scattered light intensity, confirming the presence of elongated structures for **1** also at these lower concentrations. The combined SLS and SAXS data of the aggregates formed by **1** (Supporting Information, Figure S12) were fitted to a cylindrical form factor with a length on the order of hundreds of nanometres. Thus, although both monomers form aggregates, their sizes differ considerably.

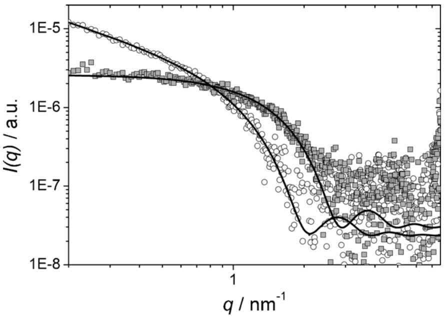

Figure 3. SAXS profiles for discotic **1** (empty circles; the fitted line is for a cylindrical form factor with $R = 1.82$ nm and $L > 52$ nm) and (*S*)-**4** (grey squares; the fitted line is for a spherical form factor with $R = 1.52$ nm). All measurements were performed in MCH with $c = 10^{-3}$ M and $T = 20$ °C.

Self-assembly mechanism of C_3-symmetrical discotic tris-amides in solution: To get more insight into the self-assembly mechanisms, we investigated the concentration-dependent ^{1}H NMR spectra of C_3-symmetrical discotic **1** in $CDCl_3$ solution (Figure 4). Chloroform is a solvent of medium polarity that limits aggregation in systems that are primarily governed by hydrogen bonding due to its competitive hydrogen-bonding character. Hence, the NMR spectra were measured at high concentration to strengthen the noncovalent interactions. In the concentration regime of 0.43–43.4 mM, the NMR spectra exhibit fast exchange between the monomeric and aggregated species. Upon increasing the concentration, significant downfield shifts are observed for the peaks corresponding to the amide proton, that is, hydrogen bonding is a crucial driving force for the self-assembly process. Moreover, slight upfield shifts of most of the peaks of the aromatic protons suggest involvement of π–π stacking interactions even in the polar chloroform environment.

The self-assembly behaviour was then investigated by means of UV/Vis and CD spectroscopy at room temperature. The spectral data were measured in MCH and chloroform to compare the aggregation behaviour in the two dif-

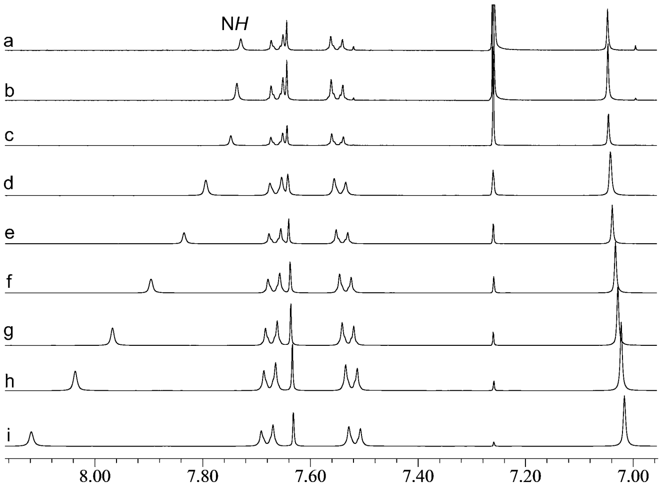

Figure 4. Partial concentration-dependent ^{1}H NMR spectra of **1** in $CDCl_3$ at different concentrations. a) 0.43, b) 0.87, c) 1.73, d) 5.20, e) 10.4, f) 16.3, g) 23.7, h) 32.6, and i) 43.4 mм. All measurements: $T=25$ °C.

ferent solvents. For the chiral compound (*S*)-**2** at a concentration of 8×10^{-6} м, no CD effect is detected in chloroform, and this suggests that (*S*)-**2** is molecularly dissolved at this concentration (Figure 5a, black line). In contrast, in MCH a bisignate Cotton effect is seen in the wavelength region between 265 and 370 nm, with a maximum at 294 nm ($\Delta\varepsilon=122\,\mathrm{L\,mol^{-1}\,cm^{-1}}$, $g=1.55\times10^{-3}$) and a minimum at 322 nm ($\Delta\varepsilon=-184\,\mathrm{L\,mol^{-1}\,cm^{-1}}$, $g=-1.95\times10^{-3}$; Figure 5a, dark grey line). This indicates a preferred helicity in the columnar aggregates formed by (*S*)-**2**, induced by the optically active (*S*)-3,7-dimethyloctyl group. As expected, a mirror-image CD spectrum is observed for enantiomer (*R*)-**3** in MCH (Figure 5a, grey line). Interestingly, the CD spectra of our N-centred OPE-based discotics are similar in size and shape to those reported for the C=O-centred OPE-based discotics,[8d] but opposite in sign when keeping the configuration of the stereogenic centre identical. This suggests that the helical preference of OPE-based discotics is governed by both the nature of the amide connectivity, which influences the conformation of the amides with respect to the π-conjugated core, and the configuration of the stereogenic centre. In fact, the importance of amide connectivity to helical bias was also found in simple alkyl-substituted BTAs, in which π–π stacking interactions are close to absent.[10d]

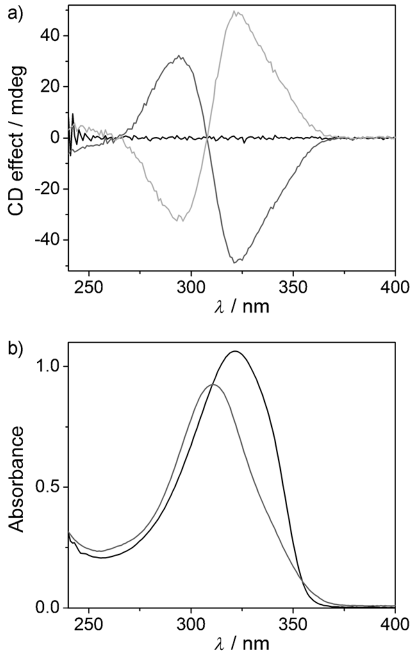

Figure 5. a) CD spectra of (*S*)-**2** (dark grey line) and (*R*)-**3** (grey line) in MCH at 20 °C. The spectrum of the molecularly dissolved state of (*S*)-**2** in chloroform is shown as well (black line). b) UV/Vis spectra for (*S*)-**2** in chloroform (black line) and MCH (grey line). All measurements: $c=8\times10^{-6}$ м.

In addition, UV/Vis spectroscopy shows that the aggregated state of (*S*)-**2** exhibits a hypsochromic shift compared to the molecularly dissolved state ($\lambda_{max}=310$ nm in MCH versus 321 nm in chloroform; Figure 5b). Such blue shift is consistent with the formation of lateral hydrogen bonds upon aggregation, which decreases the conjugation between OPE and amide groups, and indicates formation of H-type aggregates.[10a–c] Similar UV/Vis behaviour is also observed for **1**, and suggests that the achiral compound is also present in helical stacks in MCH, but now both helicities are present in equal amounts.

Temperature-dependent CD measurements were performed on chiral compound (*S*)-**2** in MCH. The temperature was slowly decreased from 70 to −10 °C at a rate of $1\,\mathrm{K\,min^{-1}}$ to ensure that the cooling was under thermodynamic control. At temperatures higher than 40 °C, the UV/Vis spectra in MCH are similar to those taken in chloroform at room temperature (Supporting Information, Figure S13), while complete disappearence of the CD intensity (Supporting Information, Figure S13) reveals a molecularly dissolved state above 40 °C. Upon further decreasing the temperature, the CD effect suddenly appears and gradually increases. Monitoring the CD intensity at $\lambda=322$ nm versus the temperature affords a non-sigmoidal melting curve, typical of a cooperative self-assembly process (Figure 6). The curve shows two regimes: one in which all molecules are molecularly dissolved (indicated by the absence of a CD effect) and an elongation regime in which the aggregate rapidly grows. Upon cooling, at a certain (concentration-dependent) temperature a large enough nucleus is formed to allow formation of an aggregate. The effect of monomer concentration on the supramolecular polymerisation process was also investigated. The temperature T_e at which the polymerisation starts gradually increases (Figure 6) with increasing concentration, suggestive of earlier formation of columnar aggregates at a higher monomer concentration.

To obtain the thermodynamic parameters for supramolecular polymerisation of (*S*)-**2**, the CD cooling curve was analysed by applying a recently developed mathematical model for supramolecular polymerisation[10j] based on equilibria between monomers, oligomers and polymers, in which the aggregation process is divided into a nucleation regime and an elongation regime. In the nucleation regime, formation of a

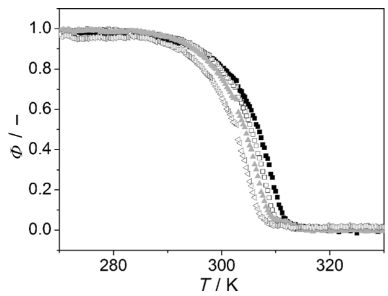

Figure 6. Net helicity Φ as a function of temperature for (*S*)-**2** in MCH probed at $\lambda = 322$ nm at four different concentrations: 1.56×10^{-5} (black closed squares), 1.03×10^{-5} (grey open squares), 8×10^{-6} (grey closed triangles) and 5.30×10^{-6} M (grey open triangles). The net helicity Φ is defined as the difference between the fraction of *M*- and *P*-type helical aggregates (net helicity = ([P]−[M])/([P]+[M])) and obtained by dividing the CD effect by the maximal attainable CD effect.

dimer, described by the equilibrium constant K_2 for dimerisation, is assumed to result in a stable nucleus. In the elongation regime, where additional monomers add to the growing polymer chain, all equilibrium constants K ($K_2 \neq K$) are assumed to be equal. As the nucleation step is highly unfavourable, $K_2 \ll K$. From non-linear least-squares analysis of the experimental melting curves, the enthalpy of elongation ΔH_e and cooperativity factor σ, defined as K_2/K and a direct measure for the cooperativity of the system, can be derived. If $\sigma = 1$, polymerisation is isodesmic (all K are equal) and increasingly small values of σ indicate an increasingly cooperative system. To improve the quality of the fit, the cooling curves measured at different concentrations were fitted simultaneously. The enthalpy release ΔH_e is around -144 kJ mol^{-1}, and σ is 3.4×10^{-3}. Interestingly, the value of ΔH_e is significantly more negative than that of the previously studied C=O-centred BTAs(-72 kJ mol^{-1}), and demonstrates the impact of enhanced π–π interactions on the thermodynamic properties of the supramolecular polymerisation process.[10j] In addition, the σ value of (*S*)-**2** is higher than that of C=O-centred BTA ($\sigma = 4.4 \times 10^{-6}$), and suggests lower cooperativity in the former case.

Additionally, fitting the natural logarithm of the dimensionless concentration (expressed as mole fraction of (*S*)-**2** in MCH) versus the reciprocal of T_e results in a modified van 't Hoff plot (Supporting Information, Figure S14) that provides an alternative method to determine the enthalpy associated with the aggregation process.[10b] The enthalpy (-182 kJ mol^{-1}, Table 2) obtained from the van 't Hoff plot further supports a considerable contribution of π–π stacking interactions to the self-assembly process.

Table 2. Self-assembly thermodynamic parameters and cooperativity factor σ of (*S*)-**2** and (*S*)-**4**. The values of ΔG and K are given at 293 K.

Compound	ΔH [kJ mol^{-1}][a]	ΔS [J mol^{-1} K^{-1}][a]	ΔG [kJ mol^{-1}][a]	K [L mol^{-1}][a]	σ[b]
(*S*)-**2**	−182	−437	−40.1	11.0×10^6	3.4×10^{-3}
(*S*)-**4**	−86	−165	−38.5	5.8×10^6	3.4×10^{-2}

[a] Calculated from modified van 't Hoff plot. [b] Derived from the equilibrium model.

Self-assembly mechanism of C_2-symmetrical discotic tris-amide in solution: Self-assembly of C_2-symmetrical discotic tris-amide (*S*)-**4** was investigated with UV and CD spectroscopy (Supporting Information, Figure S15A,B). At room temperature in dilute MCH solution, the bisignate Cotton effect of (*S*)-**4** appears in the wavelength region between 295 and 365 nm with a minimum at 316 nm ($\Delta\varepsilon = -59.0$ L mol^{-1} cm^{-1}, $g = 0.73 \times 10^{-3}$) and a maximum at 342 nm ($\Delta\varepsilon = 75.5$ L mol^{-1} cm^{-1}, $g = 1.95 \times 10^{-3}$). A pronounced red shift of around 20 nm is observed compared to (*S*)-**2**. Interestingly, we observe opposite handedness for the helical aggregates of (*S*)-**4** and (*S*)-**2**, in spite of the identical configurations of the stereogenic centres. Apparently, an amide group positioned at the centre of the molecule has a different directing effect than amide groups located at the periphery.

Temperature-dependent CD measurements at $\lambda = 342$ nm (Figure 7) display a non-sigmoidal melting curve, indicative of a cooperative supramolecular polymerisation mechanism for the C_2-symmetrical discotics. However, in the elongation stage, the slope of the curve is less steep than that of (*S*)-**2**.

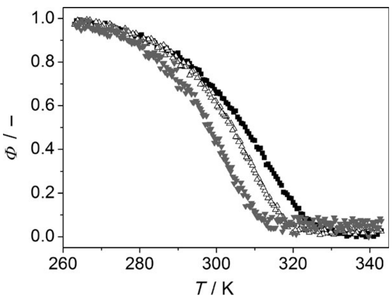

Figure 7. Net helicity Φ as a function of temperature for (*S*)-**4** in MCH probed at $\lambda = 342$ nm at three different concentrations: 1.60×10^{-5} M (black closed squares), 8×10^{-6} M (grey open triangles) and 4.00×10^{-6} M (grey closed triangles). The net helicity Φ is defined as the difference between the fraction of M- and P-type helical aggregates ([P]−[M])/([P]+[M])) and obtained by dividing the CD effect by the maximal attainable CD effect.

Since the steepness of the slope is proportional to the enthalpy release during aggregation, this is a direct reflection of weaker noncovalent interactions for the C_2-symmetrical discotics. This assumption is supported by the quantitative fitting of the normalised cooling curves ($\Delta H_e = -72$ kJ mol^{-1}, Figure 7) as well as the modified van 't Hoff plot ($\Delta H_e = -86$ kJ mol^{-1}; Supporting Information, Figure S14). The ΔH_e value is similar to those of previously reported BTAs[10j] and much lower than those of the above-discussed C_3-symmetrical discotics. On the other hand, the cooperativity factor σ is determined to be 3.4×10^{-2}, which is an order of magnitude higher than that of C_3-symmetrical analogues and implies a lower degree of cooperativity for the supramolecular polymerisation process.

The differences in stability and cooperativity in the self-assembly of C_2-and C_3-symmetrical discotics is directly connected to the differences in intermolecular hydrogen bonds and π–π stacking interactions. While the number of amide bonds is the same in both systems, the strength of the hydrogen-bonding interactions presumably is not. Previous DFT calculations on C=O-centred OPE-based discotics showed that the molecules aggregate in helical columnar stacks with adjacent molecules separated by 3.725 Å and rotated by 10°.[8d] The amide groups are twisted out of plane by around 35° to maximise the intermolecular interactions. However, the requirement for optimal intermolecular hydrogen bonding in C=O-centred BTAs are a rotation of 60° between adjacent molecules and a dihedral angle of 45° between the amide and the central benzene ring.[10d,g] Clearly, reconciling the preferred orientations of both types of intermolecular hydrogen bond in (*S*)-**4** results in a compromise, which most likely decreases the strength of the interaction. In addition, the lower number of π–π stacking interactions in the C_2-symmetrical discotics compared to the C_3-symmetrical discotics further decreases the stability of the formed aggregates. In fact, the association constant K calculated from the van 't Hoff plots (Table 2) shows a twofold reduction when the symmetry of the OPE-based discotics is decreased. This, in combination with a lower σ in (*S*)-**4** explains the differences in aggregate size between **1** and (*S*)-**4** observed in scattering studies.

Chiral amplification studies on C_3-symmetrical discotic trisamides in solution: Strategies commonly used to probe whether chiral information embedded in the molecular structure can be transferred to achieve amplification of the perceived supramolecular chirality in supramolecular assemblies are the sergeants-and-soldiers experiment and the majority-rules experiment.[14] In the sergeants-and-soldiers experiment, a small amount of chiral molecules is able to dictate the helical preference of aggregates predominantly composed of achiral compounds, which lack any preference. The majority-rules experiment refers to the ability of a small enantiomeric imbalance to dictate the handedness of helical aggregates.

The results of mixing of achiral **1** with (*S*)-**2** or (*R*)-**3** are shown in Figure 8 (the full spectra are given in Supporting Information, Figure S16A,B). Upon gradual addition of small fractions of sergeant (*S*)-**2** or (*R*)-**3** to an MCH solution of soldier **1** at a total concentration of 8.0×10^{-6} M, the shape of the CD spectra remained unchanged while the intensity exhibited a non-linear increase (Supporting Information, Figure S16A,B). The net helicity versus sergeant fraction shows mirror-image behaviour for **1**/(*S*)-**2** and **1**/(*R*)-**3** (Figure 8). In both cases, 5% of sergeant is enough to achieve the same CD effect as found for the pure chiral sergeant. This means that all helical aggregates adopt one handedness in the presence of only 5% of sergeant. This strong directing effect indicates that the randomly incorporated sergeant strongly biases the helical sense of the soldier aggregates, a direct result of the high cooperativity of this system.

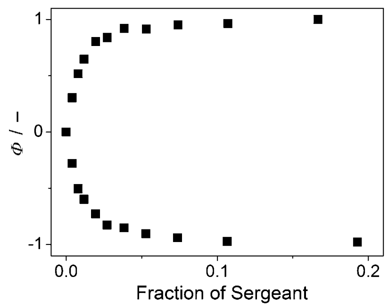

Figure 8. Net helicity Φ as a function of the sergeant fraction (*S*)-**2** and (*R*)-**3** added to **1**.

Next, majority-rules experiments were performed by mixing enantiomers (*S*)-**2** and (*R*)-**3** in different ratios at a total concentration of 8.0×10^{-6} M (see Supporting Information, Figure S16C for full spectra). The net helicity versus enantiomeric excess (*ee*) exhibits only a small deviation from linearity (Figure 9a). Such a weak majority-rules effect is not surprising when one considers the chemical structures of the monomers. The strong lateral amide hydrogen bonding and OPE π–π interactions in the core, in combination with the nine stereocentres containing methyl groups at the periphery of the monomers, significantly reduce the likelihood of mixing opposite enantiomers within one stack. In fact, similar effects have been observed previously in BTAs containing sterically demanding side chains[10i] and in porphyrin-based discotics containing 12 stereogenic centres.[3g] Additional evidence for the lack of significant mixing between (*S*)-**2** and (*R*)-**3** was gathered from measuring the cooling curves on MCH solutions of (*S*)-**2** and (*R*)-**3** at *ee* =

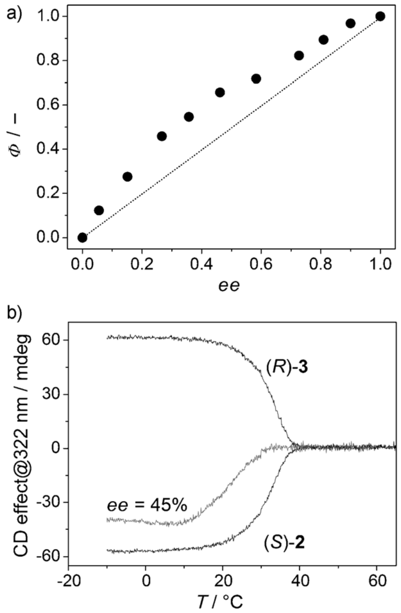

Figure 9. a) Net helicity Φ as a function of *ee* for scalemic mixtures of (*S*)-**2** and (*R*)-**3**. b) CD cooling curves of mixtures (*S*)-**2** and (*R*)-**3** with *ee* = 100, 45 and −100%.

100, 45, and −100% (Figure 9b). For the pure (*S*)-**2** and (*R*)-**3**, the elongation temperature T_e is 36.7 °C. When the *ee* value is reduced to 45%, the T_e reduces to 29.7 °C. A pronounced dependence of the T_e on the *ee* was recently theoretically predicted for helical aggregates in which the two enantiomers show high mismatch penalties, that is, there is a high energy penalty for an enantiomer to reside in a helical aggregate of its unpreferred helical sense.[10j] Thus, the 7 °C difference in T_e for $ee=100\%$ and $ee=45\%$ confirms poor mixing of opposite enantiomers in one helical stack type.

Conclusion

Novel OPE-based discotic molecules featuring C_3 and C_2 core symhttp://unabridged.merriam-webster.com/cgi-bin/unabridged?va=discotic&x=0&y=0metry were designed and synthesised to construct one-dimensional, helical, supramolecular polymers. DSC and POM measurements revealed that, in the solid state, all of the discotic compounds are crystalline and lack a columnar mesophase. We attribute this to the presence of the open π-conjugated OPE core, which for reasons of space filling and maximisation of the crystal density, does not allow formation of a columnar mesophase. IR spectroscopy shows the presence of intermolecular hydrogen bonding between neighbouring molecules, but there is no evidence for the formation of columnar structures stabilised by threefold hydrogen bonding in the solid state.

UV-Vis and CD spectroscopy on dilute MCH solutions demonstrate self-assembly into one-dimensional helical supramolecular polymers with a preferred handedness when peripheral chiral information is embedded in the side chains. One stereogenic centre suffices to fully bias the helicity in the C_2-symmetrical discotics. Self-assembly is driven by intermolecular hydrogen bonding and π–π interactions between neighbouring OPEs. From the temperature-dependent CD and UV/Vis measurements, the thermodynamic parameters characterising the self-assembly of C_3- and C_2-symmetric OPEs were derived. The core symmetry has a huge impact on the polymerisation mechanism and the stability of the formed aggregates. The C_2-symmetrical OPEs show a lower enthalpy release, a smaller association constant and a tenfold lower cooperativity compared to the C_3-symmetrical OPEs. The differing thermodynamic parameters of the C_3- and C_2-symmetrical OPEs affect the sizes of the resulting assemblies. LLS and SAXS reveal that C_3-symmetrical OPEs form long columnar structures, while C_2-symmetrical discotics form spherical aggregates at the same concentration. Chiral amplification studies on the C_3-symmetrical OPEs reveal a very strong sergeants-and-soldiers effect and a rather weak majority-rules effect.

Most importantly, the self-assembly behaviour of the C_3-symmetrical OPEs discussed here differs significantly from the OPE system recently reported by Sanchez and co-workers[8d,e] and the N- and CO-centred BTAs previously reported by us.[10b–d] We anticipate that the current results will help to understand the subtleties involved in supramolecular polymerisation processes, and benefit the future construction of more complex supramolecular aggregates. Hence, understanding the relationship between molecular structure, supramolecular polymerisation mechanism and microscopic properties of supramolecular assemblies is of crucial importance for the precise control and function of supramolecular assemblies.

Experimental Section

Materials: (*R*)-(+)-β-Citronellol and (*S*)-(−)-β-citronellol were purchased from Aldrich. 3,4,5-Trialkoxybenzoic acid was prepared according to a previously published procedure.[15] All solvents were obtained from Biosolve, except for spectrophotometric-grade methylcyclohexane and chloroform (Aldrich). All other chemicals were obtained from Acros or Aldrich. Dry dichloromethane was tapped off a distillation setup which contained molsieves. All other chemicals were used as received.

Methods: UV/Vis and CD measurements were performed on a Jasco J-815 spectropolarimeter, for which the sensitivity, time constants and scan rates were chosen appropriately. Corresponding temperature-dependent measurements were performed with a PFD-425S/15 Peltier-type temperature controller with a temperature range of 263–343 K and adjustable temperature slope; in all cases a temperature slope of 1 K min^{-1} was used. In all other measurements the temperature was set at 20 °C. In all experiments the linear dichroism was also measured, and in all cases no linear dichroism was observed. Separate UV/Vis spectra were obtained from a PerkinElmer UV/Vis spectrometer Lambda 40 at 20 °C. Cells with an optical path length of 1 cm and spectroscopic-grade solvents were employed. Solutions were prepared by weighing in the necessary amount of compound for a given concentration and transferring it to a volumetric flask. Then the flask was three-quarters filled with the spectroscopic-grade solvent and put in an oscillation bath at 40 °C for 1 h, after which the flask was allowed to cool down and filled up to its meniscus. $\Delta\varepsilon = \text{CD effect}/(32\,980 \times c \times l)$, in which c is the concentration in mol L^{-1} and l is the optical path length in cm. ^{1}H NMR and ^{13}C NMR measurements were conducted on a Varian Gemini 400 MHz. Proton chemical shifts are reported in ppm downfield from tetramethylsilane (TMS). Carbon chemical shifts are reported relative to the resonance of $CDCl_3$ as internal standard. MALDI-TOF-MS were acquired on a Perserptive Bio-system Voyager-DE PRO spectrometer. In all cases, α-cyano-4-hydroxycinnamic acid was employed as matrix material. IR spectra were recorded on a PerkinElmer spectrometer with universal ATR unit. Variable-temperature IR spectra were recorded on an Excalibur FTS 3000 MXFT-IR from Biorad. Polarisation optical microscopy was performed with a Jenaval polarisation microscope equipped with a Linkam THMS 600 heating device and crossed polarisers. The thermal transitions were determined by DSC with a PerkinElmer Pyris DSC under a nitrogen atmosphere with heating and cooling rates of 10 K min^{-1}. LLS measurements were conducted with an ALV/CGS-3 MD-4 compact goniometer system equipped with a multiple tau digital real time correlator (ALV-7004; solid-state laser: $\lambda=532$ nm, 40 mW). The observed q range was $5.5\times10^{-3} \leq q \leq 3.2\times10^{-2}$ nm^{-1}, where q is the magnitude of the scattering vector $q=(4\pi n_D/\lambda)\sin(\theta/2)$, λ the laser wavelength, n_D is the solvent refractive index and θ the scattering angle. The liquid samples were held in 5 mm borosilicate cells. The SAXS measurements were performed at the cSAXS-X12SA beamline at the Paul Scherrer Institut (PSI) in Villigen (Switzerland). SAXS images were recorded with a 2D Pilatus 2M detector with 172 × 172 μm pixel size. A sample-to-detector distance of 2.17 m was used together with an X-ray photon wavelength of 1.0 Å. The observed q range was $1.8\times10^{-1} \leq q \leq 7.6$ nm^{-1}, where q is the magnitude of the scattering vector $q=(4\pi/\lambda)\sin(\theta/2)$, λ the X-ray wavelength and θ the scattering angle The 2D images were radially averaged to obtain the intensity $I(q)$ versus q profiles. The liquid samples were held in 2 and 1 mm quartz capillaries for 10^{-4} M and 10^{-3} M samples, respectively. Standard data reduction procedures, that is, subtraction of the contributions of the empty capillary and solvent, were applied.

General procedure for the synthesis of amides 5: A solution of the appropriate trialkoxybenzoic acid (0.70 mmol), EDC (0.16 g, 0.76 mmol) and DMAP (0.055 g, 0.45 mmol) in dichloromethane (25 mL) was stirred for 1 h at room temperature, and then 4-iodoaniline (0.19 g, 0.85 mmol) was added. The reaction mixture was stirred for 24 h at room temperature, filtered, and concentrated to afford pale a yellow oil, which was washed with water and brine and then dried on $MgSO_4$. The solvent was removed in vacuo and the crude product was purified by flash column chromatography (heptane/ethyl acetate 6:1) to provide pure amides **5**.

5a: White solid (0.50 g, 82 %); ^{1}H NMR (400 MHz, $CDCl_3$, RT): $\delta = 7.68$ (s, 1H; NH), 7.66 (d, 2H; ArH), 7.41 (d, 2H; ArH), 7.01 (s, 2H; ArH), 4.02 (m, 6H; OCH_2), 1.82 (m, 6H; CH_2), 1.47 (m, 6H; CH_2), 1.20–1.38 (m, 54H; CH_2), 0.88 (t, 9H; CH_3); ^{13}C NMR (400 MHz, $CDCl_3$, RT): $\delta =$ 165.8 (C=O), 153.2 ($C_{Ar}O$), 141.5 ($C_{Ar}O$), 137.9 (C_{Ar}), 137.8 ($C_{Ar}NH$), 129.4 (C_{Ar}), 122.0 (C_{Ar}), 105.8 (C_{Ar}), 87.6 ($C_{Ar}I$), 73.6 (OCH_2), 69.4 (OCH_2), 31.9, 30.3, 29.7, 29.4, 26.1, 22.7, 14.1; MALDI-TOF MS: *m/z* 875.64 [M^+].

5b: White solid (0.42 g, 76 %); ^{1}H NMR (400 MHz, $CDCl_3$, RT): $\delta = 7.65$ (d, 2H; ArH), 7.62 (s, 1H; NH), 7.39 (d, 2H; ArH), 7.01 (s, 2H; ArH), 4.04 (m, 6H; OCH_2), 1.85 (m, 3H; CH), 1.67 (m, 6H; CH_2), 1.60 (m, 3H; CH), 1.07–1.35 (m, 18H; CH_2), 0.90 (d, 9H; CH_3), 0.84 (t, 18H; CH_3); ^{13}C NMR (400 MHz, $CDCl_3$, RT): $\delta = 165.6$ (C=O), 153.4 ($C_{Ar}O$), 141.6 ($C_{Ar}O$), 138.0 (C_{Ar}), 137.9 ($C_{Ar}NH$), 129.5 (C_{Ar}), 122.0 (C_{Ar}), 105.9 (C_{Ar}), 87.6 ($C_{Ar}I$), 71.8 (OCH_2), 67.8 (OCH_2), 39.4, 39.3, 37.5, 37.3, 36.4, 29.8, 29.7, 28.0, 24.7, 22.7, 22.6, 19.6; MALDI-TOF MS: *m/z* 791.55 [M^+].

5c: White solid (0.38 g, 69 %). All data are identical to those of **5b**.

General procedure for the synthesis of C_3-symmetrical discotic tris-amides 1–3: CuI (4.2 mg, 22 μmol), [$Pd_2(dba)_3$] (dba = *trans,trans*-dibenzylideneacetone; 13.8 mg, 15 μmol), $PtBu_3$ (60 μL, 1 mol L^{-1} in toluene, 60 μmol), diisopropylamine (100 μL, 0.70 mmol), **5** (0.40 mmol), 1,3,5-triethynylbenzene (15.0 mg, 0.10 mmol) and toluene (7 mL) were placed in flame-dried flask under Ar atmosphere. The solution was stirred overnight at room temperature and then concentrated to afford black oil, which was redissolved in chloroform. The organic layer was washed with water, 2 N aqueous HCl and brine and dried on $MgSO_4$. The solvent was removed in vacuo and the crude product was purified by flash column chromatography (heptane/chloroform/acetonitrile 5:3:1) and preparative-scale recycling GPC (chloroform as eluent) to yield C_3-symmetrical discotic tris-amides.

1: pale yellow solid (96.0 mg, 41 %); ^{1}H NMR (400 MHz, $CDCl_3$, RT): $\delta = 7.78$ (s, 3H; NH), 7.67 (s, 3H; ArH), 7.65 (d, 6H; ArH), 7.54 (d, 6H; ArH), 7.04 (s, 6H; ArH), 4.04 (m, 18H; OCH_2), 1.82 (m, 12H; CH_2), 1.75 (m, 6H; CH_2), 1.48 (m, 18H; CH_2), 1.12–1.41 (m, 162H; CH_2), 0.88 (t, 27H; CH_3); ^{13}C NMR (400 MHz, $CDCl_3$, RT): $\delta = 165.6$ (C=O), 153.3 ($C_{Ar}O$), 141.6 ($C_{Ar}O$), 138.4 ($C_{Ar}NH$), 133.8 (C_{Ar}), 132.6 (C_{Ar}), 129.6 (C_{Ar}), 124.2 (C_{Ar}), 119.9 (C_{Ar}), 118.4 (C_{Ar}), 105.7 (C_{Ar}), 90.5 (acetylene C), 87.7 (acetylene C), 73.6 (OCH_2), 69.5 (OCH_2), 31.9, 30.3, 29.7, 29.4, 26.1, 22.7, 14.1; MALDI-TOF MS: *m/z* 2393.82 [M^+].

(*S*)-2: Pale yellow solid (81.5 mg, 38 %); ^{1}H NMR (400 MHz, $CDCl_3$, RT): $\delta = 7.77$ (s, 3H; NH), 7.66 (d, 6H; ArH), 7.65 (s, 3H; ArH), 7.55 (d, 6H; ArH), 7.06 (s, 6H; ArH), 4.07 (m, 18H; OCH_2), 1.88 (m, 9H; CH), 1.71 (m, 18H; CH_2), 1.53 (m, 9H; CH), 1.12–1.39 (m, 54H; CH_2), 0.95 (d, 27H; CH_3), 0.88 (t, 54H; CH_3); ^{13}C NMR (400 MHz, $CDCl_3$, RT): $\delta =$ 165.6 (C=O), 153.5 ($C_{Ar}O$), 141.7 ($C_{Ar}O$), 138.3 ($C_{Ar}NH$), 133.7 (C_{Ar}), 132.7 (C_{Ar}), 129.6 (C_{Ar}), 124.1 (C_{Ar}), 119.7 (C_{Ar}), 118.6 (C_{Ar}), 105.7 (C_{Ar}), 90.2 (acetylene C), 87.8 (acetylene C), 71.8 (OCH_2), 67.8 (OCH_2), 39.4, 39.3, 37.5, 37.3, 36.4, 29.9, 29.7, 28.0, 24.7, 22.7, 22.6, 19.6; MALDI-TOF MS: *m/z* 2141.61 [M+H$^+$].

(*R*)-3: Pale yellow solid (75.0 mg, 35 %); ^{1}H NMR (400 MHz, $CDCl_3$, RT): $\delta = 7.75$ (s, 3H; NH), 7.68 (d, 6H; ArH), 7.65 (s, 3H; ArH), 7.55 (d, 6H; ArH), 7.06 (s, 6H; ArH), 4.08 (m, 18H; OCH_2), 1.87 (m, 9H; CH), 1.72 (m, 18H; CH_2), 1.53 (m, 9H; CH), 1.13–1.37 (m, 54H; CH_2), 0.95 (d, 27H; CH_3), 0.87 (t, 54H; CH_3); ^{13}C NMR (400 MHz, $CDCl_3$, RT): $\delta =$ 165.5 (C=O), 153.6 ($C_{Ar}O$), 141.6 ($C_{Ar}O$), 138.0 ($C_{Ar}NH$), 133.7 (C_{Ar}), 132.7 (C_{Ar}), 129.5 (C_{Ar}), 124.1 (C_{Ar}), 119.7 (C_{Ar}), 118.7 (C_{Ar}), 106.2 (C_{Ar}), 90.3 (acetylene C), 87.6 (acetylene C), 71.7 (OCH_2), 67.7 (OCH_2), 39.4, 39.3, 37.5, 37.4, 36.4, 29.9, 29.7, 28.0, 24.7, 22.7, 22.6, 19.6; MALDI-TOF MS: *m/z* 2141.60 [M+H$^+$].

Synthesis of C_2-symmetrical discotic tris-amide (*S*)-4: In a flame-dried flask under an Ar atmosphere was placed CuI (4.2 mg, 22 μmol), [$Pd_2(dba)_3$] (13.8 mg, 15 μmol), P(tBu)$_3$ (60 μL, 1 mol L^{-1} in toluene, 60 μmol), diisopropylamine (100 μL, 0.70 mmol), **5a** (250 mg, 0.28 mmol), (*S*)-2,7-dimethyloctyl-3,5-diethynylbenzamide (30.0 mg, 0.1 mmol) and toluene (7 mL). The solution was stirred overnight at room temperature and then concentrated to afford a black oil, which was redissolved in chloroform. The organic layer was washed with water, 2 N aqueous HCl and brine and dried on $MgSO_4$. The solvent was removed in vacuo, and the crude product was purified by flash column chromatography (heptane/chloroform/acetonitrile 5:3:1) and preparative-scale recycling GPC (chloroform as eluent) to yield (*S*)-**4** as a pale yellow solid (68.5 mg, 38 %). ^{1}H NMR (400 MHz, $CDCl_3$, RT): $\delta = 7.84$ (d, 2H; ArH), 7.79 (d, 1H; ArH), 7.78 (s, 2H; NH), 7.66 (d, 4H; ArH), 7.54 (d, 4H; ArH), 7.05 (s, 4H; ArH), 6.07 (t, 1H; NH), 4.04 (m, 12H; OCH_2), 3.51 (m, 2H; OCH_2), 1.83 (m, 12H; CH_2), 1.75 (m, 2H; CH), 1.49 (m, 14H; CH_2), 1.15–1.40 (m, 102H), 0.96 (d, 3H; CH_3), 0.88 (t, 24H; CH_3); ^{13}C NMR (400 MHz, $CDCl_3$, RT): $\delta = 166.1$ (C=O), 165.6 (C=O), 153.3 ($C_{Ar}O$), 141.8 ($C_{Ar}O$), 138.4 ($C_{Ar}NH$), 135.5 (C_{Ar}), 132.6 (C_{Ar}), 129.6 (C_{Ar}), 129.3 (C_{Ar}), 124.3 (C_{Ar}), 119.8 (C_{Ar}), 118.4 (C_{Ar}), 110.0 (C_{Ar}), 105.9 (C_{Ar}), 90.7 (acetylene C), 87.6 (acetylene C), 73.6 (OCH_2), 69.5 (OCH_2), 39.2, 38.4, 37.1, 36.7, 31.9, 30.8, 30.3, 29.8, 29.7, 29.6, 29.4, 28.0, 26.1, 24.7, 22.7, 22.6, 19.6, 14.1; MALDI-TOF MS: *m/z* 1805.35 [M+H$^+$].

Acknowledgements

We acknowledge financial support from the European Commission under the Seventh Framework Program by means of the grant agreement for the Integrated Infrastructure Initiative N. 262348 European Soft Matter Infrastructure (ESMI). We thank ESMI and the SLS for providing the beam time and we gratefully acknowledge technical assistance of Dr. Andreas Menzel. The authors thank Dr. Tom F. A. de Greef and Peter A. Korevaar for their valuable discussions, Rob van der Weegen for providing starting materials and Dr. Yulan Chen for the artwork. This work was supported by the European Research Council (ERC Advanced Grant No. 246829), the Dutch National Research School Combination Catalysis Controlled by Chemical Design (NRSC-Catalysis) and the Netherlands Organisation for Scientific Research (NWO - TOP Grant: 10007851).

---

[1] a) F. J. M. Hoeben, P. Jonkheijm, E. W. Meijer, A. P. H. J. Schenning, *Chem. Rev.* **2005**, *105*, 1491–1546; b) X. Feng, V. Marcon, W. Pisula, M. R. Hansen, J. Kirkpatrick, F. Grozema, D. Andrienko, K. Kremer, K. Müllen, *Nat. Mater.* **2009**, *8*, 421–426; c) A. Ciesielski, C. A. Palma, M. Bonini, P. Samori, *Adv. Mater.* **2010**, *22*, 3506–3520; d) M. Hasegawa, M. Iyoda, *Chem. Soc. Rev.* **2010**, *39*, 2420–2427.

[2] a) M. L. Bushey, T. Q. Nguyen, W. Zhang, D. Horoszewski, C. Nuckolls, *Angew. Chem.* **2004**, *116*, 5562–5570; *Angew. Chem. Int. Ed.* **2004**, *43*, 5446–5453; b) D. González-Rodríguez, A. P. H. J. Schenning, *Chem. Mater.* **2011**, *23*, 310–325.

[3] a) T. Kitahara, M. Shirakawa, S. Kawano, U. Beginn, N. Fujita, S. Shinkai, *J. Am. Chem. Soc.* **2005**, *127*, 14980–14981; b) J. Puigmartí-Luis, A. Perez del Pino, E. Laukhina, J. Esquena, V. Laukhin, C. Rovira, J. Vidal-Gancedo, A. G. Kanaras, R. J. Nichols, M. Brust, D. B. Amabilino, *Angew. Chem.* **2008**, *120*, 1887–1891; *Angew. Chem. Int. Ed.* **2008**, *47*, 1861–1865; c) S. Yagai, S. Kubota, T. Iwashima, K. Kishikawa, T. Nakanishi, T. Karatsu, A. Kitamura, *Chem. Eur. J.* **2008**, *14*, 5246–5257; d) R. Abbel, R. van der Weegen, W. Pisula, M. Surin, Ph. Leclère, E. W. Meijer, A. P. H. J. Schenning, *Chem. Eur. J.* **2009**, *15*, 9737–9746; e) N. Kumaran, P. A. Veneman, B. A. Minch, A. Mudalige, J. E. Pemberton, D. F. O'Brien, N. R. Armstrong, *Chem. Mater.* **2010**, *22*, 2491–2501; f) F. Helmich, C. C.

Lee, M. M. L. Nieuwenhuizen, J. C. Gielen, P. C. M. Christianen, A. Larsen, G. Fytas, Ph. Leclère, A. P. H. J. Schenning, E. W. Meijer, *Angew. Chem.* **2010**, *122*, 4031–4034; *Angew. Chem. Int. Ed.* **2010**, *49*, 3939–3942; g) F. Helmich, M. M. J. Smulders, C. C. Lee, A. P. H. J. Schenning, E. W. Meijer, *J. Am. Chem. Soc.* **2011**, *133*, 12238–12246.

[4] a) Y. Yamaguchi, S. Kobayashi, T. Wakamiya, Y. Matsubara, Z. Yoshida, *Angew. Chem.* **2005**, *117*, 7202–7206; *Angew. Chem. Int. Ed.* **2005**, *44*, 7040–7044; b) Y. Yamaguchi, T. Ochi, S. Miyamura, T. Tanaka, S. Kobayashi, T. Wakamiya, Y. Matsubara, Z. Yoshida, *J. Am. Chem. Soc.* **2006**, *128*, 4504–4505; c) Y. Yamaguchi, Y. Matsubara, T. Ochi, T. Wakamiya, Z. Yoshida, *J. Am. Chem. Soc.* **2008**, *130*, 13867–13869; d) R. M. Adhikari, L. Duan, L. Hou, Y. Qiu, D. C. Neckers, B. K. Shah, *Chem. Mater.* **2009**, *21*, 4638–4644.

[5] S. Höger, D. L. Morrison, V. Enkelmann, *J. Am. Chem. Soc.* **2002**, *124*, 6734–6736.

[6] a) T. L. Schull, J. G. Kushmerick, C. H. Patterson, C. George, M. H. Moore, S. K. Pollack, R. Shashidhar, *J. Am. Chem. Soc.* **2003**, *125*, 3202–3203; b) M. P. Cifuentes, C. E. Powell, J. P. Morrall, A. M. McDonagh, N. T. Lucas, M. G. Humphrey, M. Samoc, S. Houbrechts, I. Asselberghs, K. Clays, A. Persoons, T. Isoshima, *J. Am. Chem. Soc.* **2006**, *128*, 10819–10832; c) G. J. Zhou, W. Y. Wong, *Chem. Soc. Rev.* **2011**, *40*, 2541–2566; d) K. A. Green, M. P. Cifuentes, M. Samoc, M. G. Humphrey, *Coord. Chem. Rev.* **2011**, *255*, 2025–2038.

[7] U. H. F. Bunz, *Macromol. Rapid Commun.* **2009**, *30*, 772–805.

[8] a) A. Ajayaghosh, R. Varghese, S. Mahesh, V. K. Praveen, *Angew. Chem.* **2006**, *118*, 7893–7896; *Angew. Chem. Int. Ed.* **2006**, *45*, 7729–7732; b) K. Sakajiri, T. Sugisaki, K. Moriya, *Chem. Commun.* **2008**, 3447–3449; c) S. Diring, F. Camerel, B. Donnio, T. Dintzer, S. Toffanin, R. Capelli, M. Muccini, R. Ziessel, *J. Am. Chem. Soc.* **2009**, *131*, 18177–18185; d) F. Garcia, P. M. Viruela, E. Matesanz, E. Orti, L. Sanchez, *Chem. Eur. J.* **2011**, *17*, 7755–7759; e) F. Garcia, L. Sanchez, *J. Am. Chem. Soc.* **2012**, *134*, 734–742.

[9] a) D. Zhao, J. S. Moore, *Org. Biomol. Chem.* **2003**, *1*, 3471–3491; b) R. F. Service, *Science* **2005**, *309*, 95; c) A. P. H. J. Schenning, E. W. Meijer, *Chem. Commun.* **2005**, 3245–3258; d) Z. Chen, A. Lohr, C. R. Saha-Mçller, F. Wurthner, *Chem. Soc. Rev.* **2009**, *38*, 564–584; e) T. F. A. de Greef, M. J. M. Smulders, M. Wolffs, A. P. H. J. Schenning, R. P. Sijbesma, E. W. Meijer, *Chem. Rev.* **2009**, *109*, 5687–5754.

[10] a) L. Brunsveld, A. P. H. J. Schenning, M. A. C. Broeren, H. M. Janssen, J. A. J. M. Vekemans, E. W. Meijer, *Chem. Lett.* **2000**, 292–293; b) M. M. J. Smulders, A. P. H. J. Schenning, E. W. Meijer, *J. Am. Chem. Soc.* **2008**, *130*, 606–611; c) P. J. M. Stals, M. M. J. Smulders, R. Martin-Rapun, A. R. A. Palmans, E. W. Meijer, *Chem. Eur. J.* **2009**, *15*, 2071–2080; d) P. J. M. Stals, J. C. Everts, R. de Bruijn, I. A. W. Filot, M. M. J. Smulders, R. Martin-Rapun, E. A. Pidko, T. F. A. de Greef, A. R. A. Palmans, E. W. Meijer, *Chem. Eur. J.* **2010**, *16*, 810–821; e) M. M. J. Smulders, I. A. W. Filot, J. M. A. Leenders, P. van der Schoot, A. R. A. Palmans, A. P. H. J. Schenning, E. W. Meijer, *J. Am. Chem. Soc.* **2010**, *132*, 611–619; f) M. M. J. Smulders, P. J. M. Stals, T. Mes, T. F. E. Paffen, A. P. H. J. Schenning, A. R. A. Palmans, E. W. Meijer, *J. Am. Chem. Soc.* **2010**, *132*, 620–626; g) I. A. W. Filot, E. A. Pidko, A. R. A. Palmans, E. W. Meijer, R. A. van Santen, T. F. A. de Greef, *J. Phys. Chem. A J. Phys. Chem. B.* **2010**, *114*, 13667–13674; h) S. Cantekin, D. W. R. Balkenende, M. M. J. Smulders, A. R. A. Palmans, E. W. Meijer, *Nat. Chem.* **2011**, *3*, 42–46; i) M. A. J. Veld, D. Haveman, A. R. A. Palmans, E. W. Meijer, *Soft Matter* **2011**, *7*, 524–531; j) A. J. Markvoort, H. M. M. ten Eikelder, P. A. J. Hilbers, T. F. A. de Greef, E. W. Meijer, *Nat. Commun.* **2011**, *2*, 509.

[11] a) J. A. Rego, S. Kumar, I. J. Dmochowski, H. Ringsdorf, *Chem. Commun.* **1996**, 1031–1032; b) E. J. Foster, J. Babuin, N. Nguyen, V. E. Williams, *Chem. Commun.* **2004**, 2052–2053; c) X. Feng, W. Pisula, T. Kudernac, D. Wu, L. Zhi, S. De Feyter, K. Mullen, *J. Am. Chem. Soc.* **2009**, *131*, 4439–4448; d) M. A. J. Gillissen, T. T. Hoeben, A. J. H. Spiering, J. A. J. M. Vekemans, A. R. A. Palmans, E. W. Meijer, *Isr. J. Chem.* **2011**, *51*, 1118–1127.

[12] A. Soheili, J. Albaneze-Walker, J. A. Murry, P. G. Dormer, D. L. Hughes, *Org. Lett.* **2003**, *5*, 4191–4194.

[13] L. Chen, J. Kim, T. Ishizuka, Y. Honsho, A. Saeki, S. Seki, H. Ihee, D. Jiang, *J. Am. Chem. Soc.* **2009**, *131*, 7287–7292.

[14] A. R. A. Palmans, E. W. Meijer, *Angew. Chem.* **2007**, *119*, 9106–9126; *Angew. Chem. Int. Ed.* **2007**, *46*, 8948–8968.

[15] S. Ghosh, X. Q. Li, V. Stepanenko, F. Wurthner, *Chem. Eur. J.* **2008**, *14*, 11343–11357.

Received: March 15, 2012
Revised: May 11, 2012

Helical supramolecular polymers: Discotic compounds with C_3 or C_2 core symmetry were designed and synthesised to construct oligo(phenylene-ethynylene)-based one-dimensional helical supramolecular polymers. A remarkable influence of core symmetry on the thermodynamic parameters of the supramolecular polymerisation process is demonstrated, which affects the size of the resulting aggregates (see figure).

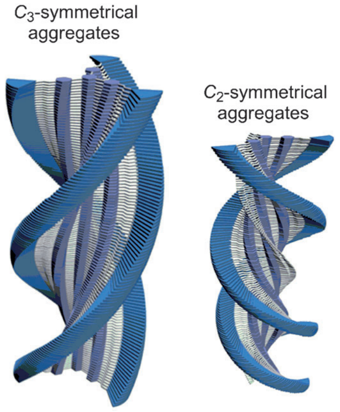

Supramolecular Chemistry

F. Wang, M. A. J. Gillissen,
P. J. M. Stals, A. R. A. Palmans,*
E. W. Meijer* .... ▮▮▮▮–▮▮▮▮

Hydrogen Bonding Directed Supramolecular Polymerisation of Oligo(Phenylene-Ethynylene)s: Cooperative Mechanism, Core Symmetry Effect and Chiral Amplification